International Journal of GEOMATE, May, 2026 Vol.30, Issue 141, pp.67-74
ISSN: 2186-2982 (P), 2186-2990 (O), Japan, DOI: https://doi.org/10.21660/2026.141.5473
Geotechnique, Construction Materials and Environment

EXACT SHAPE FUNCTIONS AND DISPLACEMENT FIELDS FOR NON-PRISMATIC EULER-BERNOULLI BEAMS DERIVED FROM GOVERNING DIFFERENTIAL EQUATIONS

Nghia Hieu Hoang[1], *Khiem Van Giang[2] and Hien Manh Nghiem[2]

[1]Faculty of Technology and Engineering, Haiphong University, Vietnam; [2]Department of Civil Engineering, Hanoi Architectural University, Vietnam

*Corresponding Author, Received: 05 Feb. 2026, Revised: 16 Mar. 2026, Accepted: 24 Mar. 2026

ABSTRACT: This study presents an exact analytical formulation for the deflection response of non-prismatic Euler-Bernoulli beams with continuously varying flexural rigidity. Starting from the classical beam assumptions, the governing differential equation with variable coefficients is derived and solved directly for a general power-law representation of stiffness variation along the beam axis. A load-potential decomposition is introduced to decouple the contribution of external loading from the homogeneous displacement field, allowing a unified and exact treatment of uniformly distributed loads, concentrated loads, and partially applied loads within a single analytical framework. Based on the resulting homogeneous solution space, exact shape functions are constructed by enforcing nodal compatibility and boundary conditions, ensuring pointwise satisfaction of equilibrium without resorting to assumed polynomial interpolation. Closed-form expressions for displacements are obtained for both cantilever and simply supported beams. The analytical solutions are verified through numerical comparisons with finite-element results obtained using a discretized representation of the non-prismatic beam, showing excellent agreement across all loading cases. The proposed formulation provides a rigorous analytical benchmark for non-prismatic beam behavior and offers a reliable reference for the verification and development of numerical and finite-element beam models with variable stiffness.

Keywords: Euler-Bernoulli beam; Non-prismatic beam; Displacement field; Shape function;

1. INTRODUCTION

Non-prismatic (tapered) beam members are widely used in civil, mechanical, and structural engineering applications due to their efficient material utilization, improved strength-to-weight ratio, and architectural flexibility. Typical examples include bridge girders, crane booms, towers, frames with variable depth, and vibration-sensitive structural components. In such members, the cross-sectional properties vary continuously along the beam axis, resulting in spatially varying stiffness and mass distributions. Consequently, their structural response differs fundamentally from that of prismatic beams, and accurate analysis requires formulations that properly account for these variations.

Classical studies have demonstrated that Euler-Bernoulli beam theory provides an accurate description of the bending response of slender beams with smoothly varying cross-sections [1]. These works focused on assessing the validity of the classical assumptions by directly examining the governing differential equations and, in some cases, by comparing the leading-order beam solutions with more refined analytical treatments.

Eisenberger [2] derived explicit stiffness matrices for several classes of non-prismatic members by first formulating exact flexibility coefficients and then inverting the flexibility matrix. This approach avoided discretizing tapered members into multiple prismatic elements and significantly reduced computational effort while maintaining accuracy. Numerical comparisons showed that conventional sectional subdivision requires a large number of elements to achieve comparable precision, particularly for strongly tapered members. Similarly, Banerjee and Williams [3] derived exact Bernoulli-Euler static stiffness matrices for tapered beam-columns by solving the governing differential equations using Bessel functions for selected taper laws. Although their formulation provided highly accurate stiffness expressions, it was restricted to specific functional forms of sectional variation and relied on special functions, which complicates extension to general stiffness profiles and implementation in standard finite-element frameworks.

Other researchers focused on displacement-based finite-element formulations for tapered beams. Tang [4] classified different types of tapered beam-columns and proposed interpolation functions based on assumed polynomial displacement fields, while Shooshtari and Khajehdezfuly [5] investigated static responses using refined finite-element formulations. Although these approaches improved accuracy compared with uniform beam models, most relied on assumed displacement interpolations that do not satisfy the governing differential equation exactly.

To enhance numerical performance, force-based and mixed finite-element formulations have also been

proposed. Valipour and Bradford [6] developed a force interpolation method for tapered three-dimensional beam elements with flexible connections, demonstrating superior convergence compared with conventional Hermitian interpolation. Soltani et al. [7] presented a finite-element formulation for the stability and free-vibration analysis of non-prismatic thin-walled beams based on Timoshenko beam theory, employing numerical integration to evaluate stiffness and mass matrices for members with continuously varying cross-sectional properties. While this formulation captures warping, shear deformation, and geometric variation effectively, it relies on numerical discretization and does not yield closed-form displacement fields or shape functions.

More recently, Auricchio et al. [8] developed a mixed variational formulation and corresponding finite-element model for linearly elastic non-prismatic beams, with the objective of improving stress accuracy and enforcing boundary equilibrium within the small-deformation regime. Ibrahim et al. [9] investigated the free vibration behavior of tapered beams and plates using a unified beam theory bridging Euler–Bernoulli and Timoshenko formulations. Although these studies provide accurate numerical predictions, the resulting formulations typically rely on numerical solution procedures and closed-form shape functions or analytical stiffness matrices are generally not available.

Despite the extensive body of research, most existing formulations for non-prismatic beams continue to rely on assumed polynomial interpolation, numerical approximation of the governing equations, or load-specific solution procedures. As a result, solution accuracy depends strongly on mesh refinement or higher-order interpolation. Motivated by these limitations, the present study develops an exact formulation for non-prismatic Euler-Bernoulli beams by deriving the displacement field directly from the governing differential equation.

The novelty of this work lies in the combination of a general power-law stiffness representation, a load-potential decomposition for unified load treatment, and a displacement-first derivation of exact shape functions valid for arbitrary exponent n. Earlier exact stiffness-based approaches typically derive element stiffness matrices through flexibility inversion. In contrast, the present formulation derives the displacement field directly from the governing differential equation, leading to explicit closed-form displacement expressions and shape functions. These analytical expressions provide transparent benchmarks for validating numerical and finite-element solutions. Furthermore, the formulation offers a systematic framework for analyzing non-prismatic beams with continuously varying stiffness without relying on assumed interpolation functions.

2. RESEARCH SIGNIFICANCE

This study presents an exact analytical formulation for non-prismatic Euler–Bernoulli beams derived directly from the governing differential equation. Unlike conventional approaches based on assumed polynomial interpolation, the proposed method constructs the displacement field from the exact solution space of the variable-stiffness beam equation, ensuring pointwise satisfaction of equilibrium and compatibility. A load-potential decomposition is introduced to separate the effects of external loading from the homogeneous displacement field, allowing uniform, concentrated, and partial loads to be treated within a unified and load-independent framework. Based on the homogeneous solution, exact shape functions are derived by enforcing nodal compatibility. The resulting formulation provides a rigorous analytical benchmark for the displacement response of tapered beam members and a reliable foundation for validating numerical and finite-element models in structural engineering applications.

3. GOVERNING EQUATIONS

The solution procedure follows four main steps: (1) derive the governing differential equation for variable flexural rigidity; (2) integrate the equation to obtain the general displacement field composed of homogeneous and load-dependent parts; (3) enforce boundary conditions to determine integration constants; (4) construct exact shape functions by expressing the constants in terms of nodal degrees of freedom.

3.1 Differential Equations

The formulation presented in this study is based on the classical Euler–Bernoulli beam theory. The beam is assumed to be slender, homogeneous, and linearly elastic, with small deformations such that geometric nonlinearity is neglected. Plane cross-sections are assumed to remain plane and perpendicular to the deformed beam axis, and shear deformation effects are not considered, and the analysis focuses on the bending response [10,11]. The moment of inertia is positive and varies continuously along the beam axis and is represented by a power-law function of the longitudinal coordinate. Material properties are assumed constant within each cross-section. External loads act in the transverse direction and may vary along the beam length, while body forces are neglected and only static loading is considered.

For an Euler–Bernoulli beam with variable flexural rigidity, the bending moment-curvature relationship is expressed as:

$$M(x) = EI(x)\, w''(x) \quad (1)$$

where E is Young's modulus of the beam material; $I(x)$ is moment of inertia of the beam cross section; $M(x)$ is bending moment along the beam axis; and $w''(x)=\phi(x)$ is curvature; $w(x)$ is the transverse displacement.

Considering free-body diagram of an infinitesimal beam element in Fig. 1, the following equations can be obtained:

$$V'(x) = q(x) \quad (2a)$$

$$M'(x) = V(x) \quad (2b)$$

The equilibrium equation under transverse loading $q(x)$ determined from Eq. (2) is:

$$M''(x) = q(x) \quad (3)$$

Combining Eqs. (1) and (2) yields the governing differential equation:

$$[EI(x)\, w''(x)]'' = q(x) \quad (4)$$

Integrating twice with respect to x yields:

$$EI(x)w''(x) = \int\int q(x)dx\,dx + C_1x + C_2 \quad (5a)$$

or

$$w''(x) = \frac{f_q(x)}{EI(x)} + \frac{C_1x+C_2}{EI(x)} \quad (5b)$$

where:

$$f_q(x) = \int\int q(x)dx\,dx \quad (5c)$$

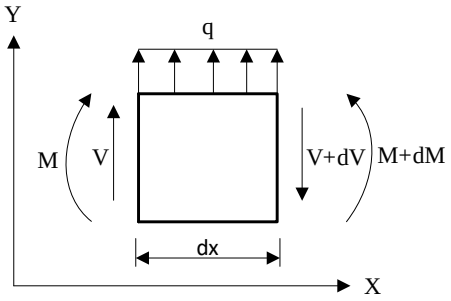

Fig. 1 Free-body diagram of an infinitesimal beam element

3.2 Cross Section Variation

In this study, the moment of inertia is assumed to be power law along the beam axis [12]:

$$I(x) = \left(\frac{\sqrt[n]{I_1}-\sqrt[n]{I_0}}{L}x + \sqrt[n]{I_0}\right)^n = (Ax+B)^n \quad (6)$$

where I_0 and I_1 are moments of inertia at the first and second ends of the beam; n is power law of moment of inertia variation; $A = \frac{\sqrt[n]{I_1}-\sqrt[n]{I_0}}{L}$ and $B = \sqrt[n]{I_0}$.

This form is sufficiently general to represent tapered beam sections and ensures analytical integrability of the governing equation.

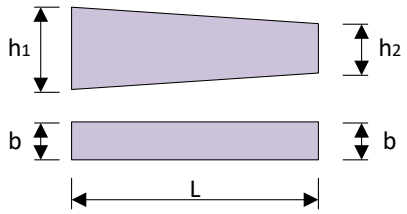

Fig. 2 Non-prismatic rectangular beam with section height varies linearly along the beam

Considering the non-prismatic beam with a rectangular cross-section shown in Fig. 2 with h_1=0.4m, b=0.2m, h_2=1.0m, the variation of the moment of inertia resulting from a linear change in the section height along the beam is illustrated in Fig. 3. The corresponding approximation using Eq. (6) with n=3 is also shown, demonstrating excellent agreement with the exact inertia distribution. For the beam with both the width and height vary linearly along the beam as shown in Fig. 4 (h_1=0.4m, b_1=0.2m, h_2=1.0m, b_2=0.4m), the variation of the moment of inertia is presented in Fig. 5. In this case, the best fit of Eq. (6) is achieved by adopting n=4.

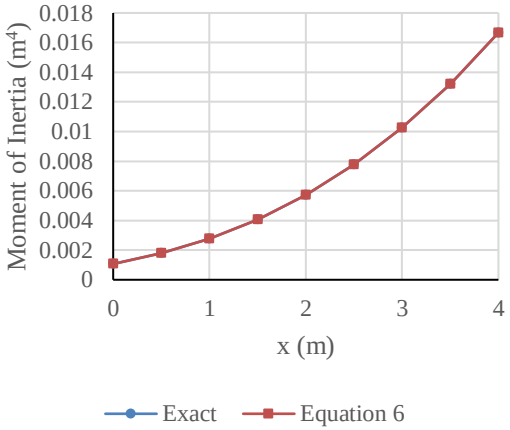

Fig. 3 Moment of inertia for n=3

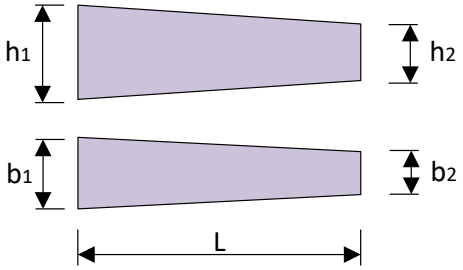

Fig. 4 Non-prismatic rectangular beam with section height and width vary linearly along the beam

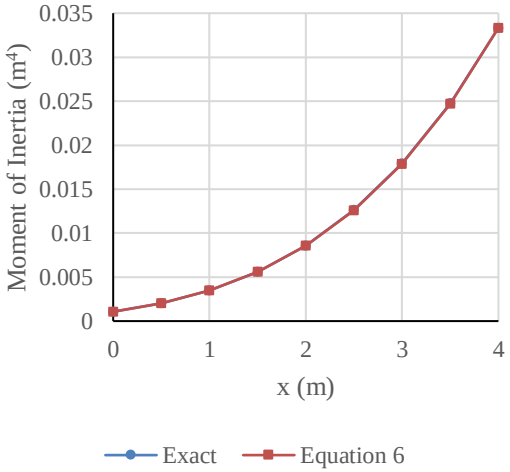

Fig. 5 Moment of inertia for n=4

3.3 Solution of Differential Equations

The above expression clearly separates the particular solution, governed by the applied load $q(x)$, from the homogeneous solution, governed by the internal force parameters C_1 and C_2. This separation allows the displacement field to be constructed systematically by integrating each term independently. Integrating the curvature field twice of Eq. (5) gives the transverse displacement:

$$w(x) = C_4 + C_3 x + \Phi_f(x) + C_1\Phi_1(x) + C_2\Phi_0(x) \quad (7)$$

where C_3 and C_4 correspond to the displacement and rotation at the reference end and:

$$\Phi_0(x) = \int_0^x \int_0^\xi \frac{1}{(At+B)^n}\, dt\, d\xi \quad (8a)$$

$$\Phi_1(x) = \int_0^x \int_0^\xi \frac{t}{(At+B)^n}\, dt\, d\xi \quad (8b)$$

$$\Phi_f(x) = \int_0^x \int_0^\xi \frac{f_q(t)}{(At+B)^n}\, dt\, d\xi \quad (8c)$$

For n=3:

$$\Phi_0(x) = \frac{x^2}{2B^2(Ax+B)} \quad (9a)$$

$$\Phi_1(x) = \frac{x}{2A^2B} + \frac{1}{A^3}\left[-\ln\left(\frac{Ax+B}{B}\right) + \frac{1}{2}\left(1-\frac{B}{Ax+B}\right)\right] \quad (9b)$$

For n=4:

$$\Phi_0(x) = \frac{x^2(2Ax+3B)}{6B^3(Ax+B)^2} \quad (10a)$$

$$\Phi_1(x) = \frac{x}{6A^2B^2} + \frac{1}{A^3}\left(-\frac{1}{3B} + \frac{1}{2(Ax+B)} - \frac{B}{6(Ax+B)^2}\right) \quad (10b)$$

Function $\Phi_f(x)$ can be obtained as follows:

Beam under uniform load

$$\Phi_f(x) = q\int_0^x \int_0^\xi \frac{t^2}{2EI(t)}\, dt\, d\xi \quad (11a)$$

For n=3:

$$\Phi_f(x) = \frac{q}{2EI_0A^4}\left[(Ax+3B)\ln\left(\frac{Ax+B}{B}\right) - \frac{5}{2}Ax + \frac{B^2}{2(Ax+B)} - \frac{B}{2}\right] \quad (11b)$$

For n=4:

$$\Phi_f(x) = \frac{q}{2EI_0A^4}\left[-\ln\left(\frac{Ax+B}{B}\right) + B\left(\frac{1}{B} - \frac{1}{Ax+B}\right) + \frac{B^2}{6}\left(\frac{1}{(Ax+B)^2} - \frac{1}{B^2}\right) + \frac{Ax}{3B}\right] \quad (11c)$$

Beam under point load

The equivalent distributed load can be obtained as:

$$q(x) = P\,\delta(x-d) \quad (12)$$

where $\delta(\cdot)$ denotes the Dirac delta function.

Load function for point load:

$$f_q(x) = P(x-d)H(d-x) \quad (13)$$

where $H(\cdot)$ is the Heaviside function.

Thus:

$$\Phi_f(x) = P\int_0^x \int_0^\xi \frac{(t-L)H(L-t)}{EI(t)}\, dt\, d\xi \quad (14a)$$

For n=3:

$$\Phi_f(x) = \frac{P\,H(x-d)}{2EI_0A^3(Ax+B)(Ad+B)}\left[(Ax+B)^2 - (Ad+B)^2 - 2(Ax+B)(Ad+B)\ln\left(\frac{Ax+B}{Ad+B}\right)\right] \quad (14b)$$

For n=4:

$$\Phi_f(x) = \frac{P\,H(x-d)\,(x-d)^3}{6EI_0(Ad+B)^2(Ax+B)^2} \quad (14c)$$

This formulation ensures that the governing differential equation is satisfied exactly, while the boundary conditions are enforced explicitly through the integration constants. The approach avoids assumed polynomial interpolation and provides a consistent foundation for deriving shape functions, stiffness matrices, and load vectors for non-prismatic beam elements.

4. APPLICATION OF THE DERIVED FORMULATION

The present formulation is general and can be applied to beams with arbitrary boundary conditions provided that four independent boundary conditions are available to determine the integration constants. Exact shape functions, analyses of cantilever and simply supported beams are used here as representative benchmark cases.

4.1 Exact Shape Functions

The shape functions represent the interpolation of the transverse displacement field within a beam element and are obtained directly from the closed-form solution of the governing differential equation. The shape functions serve as a rigorous analytical basis for reconstructing deflection curves, validating numerical models and forming stiffness and mass matrices, and load vector etc. in the finite element method.

For a beam element of length L with nodal DOFs as shown in Fig. 6:

$$\{w_1, \phi_1, w_2, \phi_2\} \quad (15)$$

The boundary conditions are:

$$w(0) = w_1;\ \theta(0) = \theta_1 \quad (16a)$$

$$w(L) = w_2;\ \theta(L) = \theta_2 \quad (16b)$$

At $x = 0$:

$$C_3 = \theta_1 \text{ and } C_4 = w_1 \quad (17a)$$

At $x = L$:

$$w_2 = w_1 + \theta_1 L + C_1\Phi_1(L) + C_2\Phi_0(L) \quad (17b)$$

$$\theta_2 = \theta_1 + C_1\Phi_1'(L) + C_2\Phi_0'(L) \quad (17c)$$

Solving Eq. (13) yields:

$$C_1 = \frac{(w_2 - w_1 - \theta_1 L)\,\Phi_0'(L) - (\theta_2 - \theta_1)\,\Phi_0(L)}{\Delta} \quad (18a)$$

$$C_2 = \frac{(\theta_2 - \theta_1)\,\Phi_1(L) - (w_2 - w_1 - \theta_1 L)\,\Phi_1'(L)}{\Delta} \quad (18b)$$

where:

$$\Delta = \Phi_1(L)\Phi_0'(L) - \Phi_0(L)\Phi_1'(L) \quad (19)$$

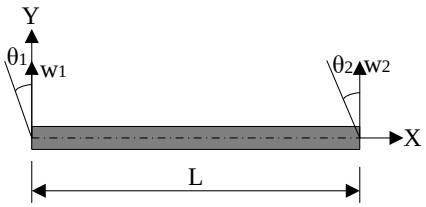

Fig. 6 Nodal displacements

The displacement field becomes:

$$w(x) = N_1(x)w_1 + N_2(x)\theta_1 + N_3(x)w_2 + N_4(x)\theta_2 \quad (20)$$

where:

$$N_1(x) = 1 - \frac{\Phi_1(x)\Phi_0'(L) - \Phi_0(x)\Phi_1'(L)}{\Delta}$$

$$N_2(x) = x - \frac{L[\Phi_1(x)\Phi_0'(L) - \Phi_0(x)\Phi_1'(L)]}{\Delta} + \frac{\Phi_1(x)\Phi_0(L) - \Phi_0(x)\Phi_1(L)}{\Delta} \quad (21)$$

$$N_3(x) = \frac{\Phi_1(x)\Phi_0'(L) - \Phi_0(x)\Phi_1'(L)}{\Delta}$$

$$N_4(x) = \frac{\Phi_0(x)\Phi_1(L) - \Phi_1(x)\Phi_0(L)}{\Delta}$$

Fig. 7 illustrates the derived shape functions N_1–N_4 along the beam span. The functions satisfy the essential interpolation requirements, with N_1 and N_3 governing transverse displacement compatibility and N_2 and N_4 associated with rotational degrees of freedom. The derived shape functions can be readily incorporated into standard finite-element beam formulations following conventional element assembly procedures.

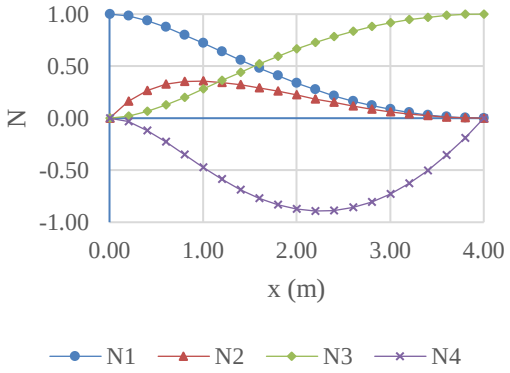

Fig.7 Shape functions of the non-prismatic beam

4.2 Deflection of the non-prismatic cantilever beam

Under uniform load

The beam is fixed at $x = 0$, free at $x = L$ and under uniform load q only as shown in Fig. 8. The boundary conditions can be obtained as:

$$w(0) = 0, \theta(0) = 0, M(L) = 0, V(L) = 0 \quad (22)$$

From free-end conditions:

$$V(L) = qL + C_1 = 0 \Rightarrow C_1 = -qL \quad (23)$$

$$M(L) = \frac{q}{2}L^2 + C_1 L + C_2 = 0 \Rightarrow C_2 = \frac{q}{2}L^2 \quad (24)$$

From fixed-end conditions:

$$C_3 = 0 \text{ and } C_4 = 0 \quad (25)$$

Displacement equation:

$$w(x) = \Phi_f(x) - qL\Phi_1(x) + \frac{q}{2}L^2\Phi_0(x) \quad (26)$$

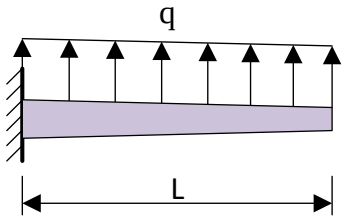

Fig. 8 Cantilever beam under uniform load

Under point load at the tip

The beam is under point load P applied at the tip, as shown in Fig. 9, cantilever at $x = 0$, free at $x = L$. The boundary conditions can be obtained as:

$$w(0) = 0, w'(0) = 0, M(L) = 0, V(L) = P \quad (27)$$

From equilibrium at the free end:

$$C_1 = -P, C_2 = PL \quad (28)$$

and from the fixed end:

$$C_3 = 0 \text{ and } C_4 = 0 \quad (29)$$

The displacement field can be expressed as:

$$w(x) = \Phi_f(x) - P\,\Phi_1(x) + PL\,\Phi_0(x) \quad (30)$$

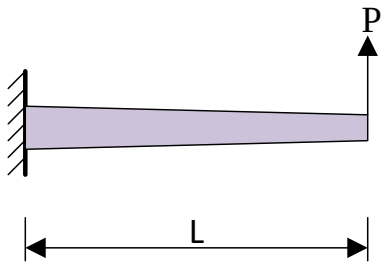

Fig. 9 Cantilever beam under point load

Numerical examples

The beams considered are illustrated in Figs. 8 and 9. A constant Young's modulus of $E = 30$MPa is assumed for all cases, and the beams have rectangular cross sections and length of L=4m. Two non-prismatic beam configurations are analyzed. In Case 1, the beam height varies linearly along the span while the width remains constant. The cross-sectional dimensions at the fixed and free ends are $h_1 = 1.0$m, $b_1 = 0.2$m, $h_2 = 0.4$m, and $b_2 = 0.2$m, resulting in a cubic variation of the second moment of area along the beam length ($n = 3$). In Case 2, both the height and width vary linearly along the beam. The corresponding dimensions are $h_1 = 1.0$ m, $b_1 = 0.4$m at the fixed end and $h_2 = 0.4$m, $b_2 = 0.2$m at the free end, leading to a quartic variation of the flexural rigidity ($n = 4$). The point load is applied at the tip of the beam (d=4m). The analytical displacement solutions derived in this study are validated against numerical results obtained using the KCW structural analysis program. In the KCW model, the non-prismatic beam is discretized into sixteen

prismatic beam elements. Each element is assigned a constant flexural stiffness evaluated at its midpoint to approximate the continuously varying stiffness.

Figs. 10 through 13 present comparisons of the deflection curves for cantilever beams subjected to uniformly distributed loads and concentrated tip loads. Excellent agreement is observed between the proposed closed-form solution and the KCW numerical results. Minor discrepancies near the free end are attributed to the stepped approximation of stiffness in the numerical model. The differences in maximum displacement are small, as summarized in Table 1.

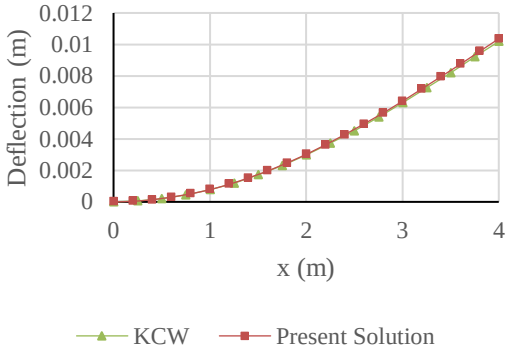

Fig. 10 Deflection of cantilever beam under uniform load for n=3

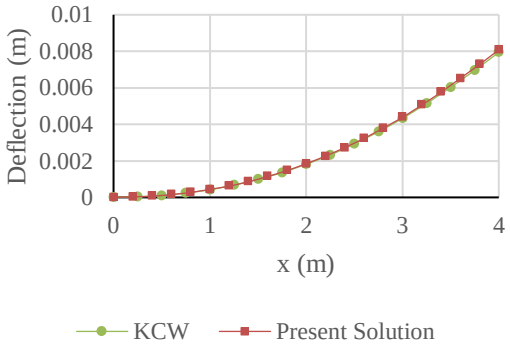

Fig. 11 Deflection of cantilever beam under point load for n=3

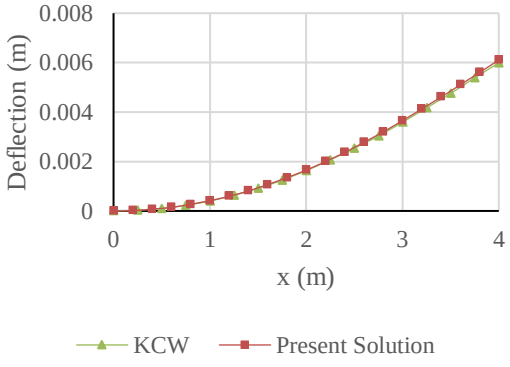

Fig. 12 Deflection of cantilever beam under uniform load for n=4

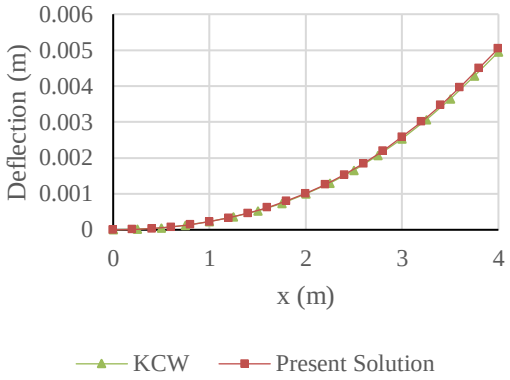

Fig. 13 Deflection of cantilever beam under point load for n=4

Table 1. Maximum displacements of cantilever beam (m)

Case	Present Solution	KCW	Difference (%)
1 (n=3)	0.010361	0.010186	1.69
2 (n=3)	0.008076	0.007938	1.71
1 (n=4)	0.006108	0.005995	1.85
2 (n=4)	0.005044	0.004947	1.92

4.3 Deflection of the non-prismatic simply supported beam

The simply supported beam is supported at $x = 0$ and $x = L$, as shown in Figs. 14 and 15. The typical boundary conditions are:

$$w(0) = 0, w(L) = 0, M(0) = 0, M(L) = 0 \quad (31)$$

Under uniform load

In Fig. 14, the beam is under uniform load q. From $M(0) = 0$:

$$C_2 = 0 \quad (32)$$

From $M(L) = 0$:

$$\frac{q}{2}L^2 + C_1 L = 0 \Rightarrow C_1 = -\frac{q}{2}L \quad (33)$$

From $w(0) = 0$:

$$C_4 = 0 \quad (34)$$

From $w(L) = 0$:

$$C_3 = -\frac{1}{L}\left[\Phi_f(L) - \frac{qL}{2}\Phi_1(L)\right] \quad (35)$$

The deflection of the beam under uniform load is expressed as:

$$w(x) = \Phi_f(x) - \frac{qL}{2}\Phi_1(x) - \frac{x}{L}\left[\Phi_f(L) - \frac{qL}{2}\Phi_1(L)\right] \quad (36)$$

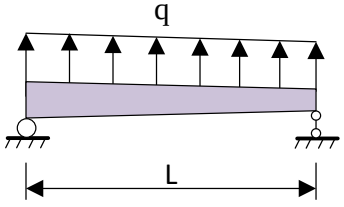

Fig. 14 Simply supported beam under uniform load

Under a point load at x=d

The beam is under a point load P as shown in Fig. 15. From $M(0) = 0$ and $M(L) = 0$:

$$C_2 = 0 \quad (37)$$

$$C_1 = -\frac{P(L-d)}{L} \quad (38)$$

From displacement conditions $w(0)=0$ and $w(L)=0$:

$$C_4 = 0 \quad (39)$$

$$C_3 = -\frac{\Phi_f(L)+C_1\Phi_1(L)}{L} \quad (40)$$

The deflection of the beam under point load is obtained as:

$$w(x) = \Phi_f(x) - \frac{(L-d)P}{L}\Phi_1(x) - \frac{x}{L}[\Phi_f(L) + \frac{(L-d)P}{L}\Phi_1(L)] \quad (41)$$

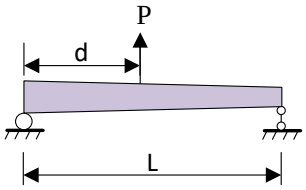

Fig. 15 Simply supported beam under point load

Numerical examples

The simply supported beams illustrated in Figs. 15 and 16 are also analyzed. The material properties and cross-sectional configurations are identical to those adopted for the cantilever beam cases. The point load is applied at mid-point of the beam (d=2 m). Two non-prismatic cross-section scenarios are considered, corresponding to cubic ($n = 3$) and quartic ($n = 4$) variations of the flexural rigidity along the beam length.

The results demonstrate the capability of the proposed analytical formulation to accurately predict the deflection behavior of simply supported non-prismatic beams. The present solution shows excellent agreement with the numerical results obtained using the KCW program, as illustrated in Figs. 16 through 19. The differences in maximum displacement remain small, ranging from approximately 1.68% to 2.37%, as summarized in Table 2. These minor discrepancies are primarily attributed to the piecewise-constant approximation of flexural stiffness inherent in the KCW discretization rather than any limitation of the analytical displacement formulation.

Table 2. Maximum displacements of simply supported beam (m)

Case	Present Solution	KCW	Difference (%)
1 (n=3)	0.002305	0.002266	1.69
2 (n=3)	0.000893	0.000878	1.68
1 (n=4)	0.001688	0.001648	2.37
2 (n=4)	0.000641	0.000629	1.84

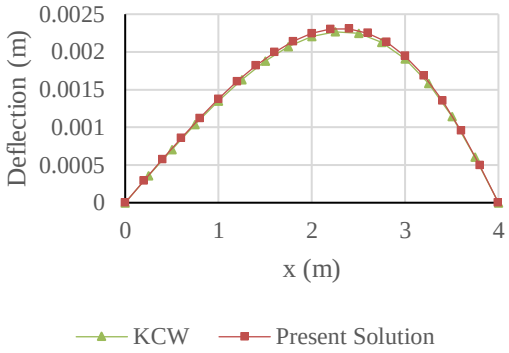

Fig. 16 Deflection of simply supported beam under uniform load for n=3

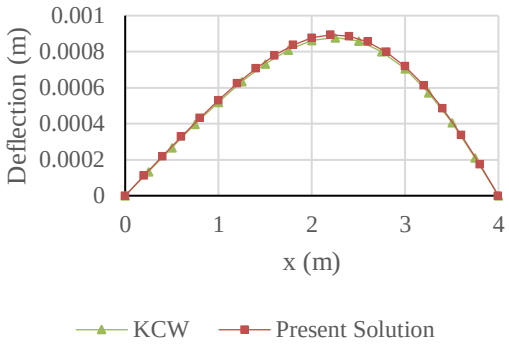

Fig. 17 Deflection of simply supported beam under point load for n=3

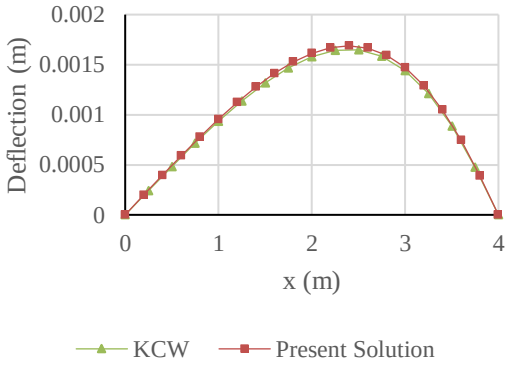

Fig. 18 Deflection of simply supported beam under uniform load for n=4

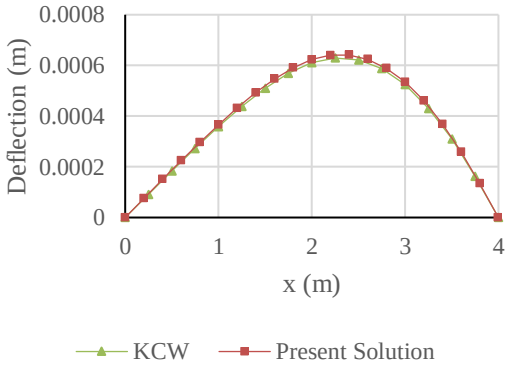

Fig. 19 Deflection of simply supported beam under point load for n=4

5. CONCLUSIONS

This study presented an analytical formulation for the displacement response of non-prismatic Euler–Bernoulli beams with continuously varying flexural rigidity. By representing the stiffness variation using a general power-law function and solving the governing differential equation directly, closed-form displacement expressions were obtained without relying on assumed polynomial interpolation or sectional discretization. A load-potential function was introduced to separate the effects of external loading from the homogeneous displacement field, enabling a unified treatment of uniformly distributed loads, concentrated forces, and partial loading conditions.

Based on the homogeneous displacement solution, exact shape functions were derived by enforcing nodal compatibility conditions so that equilibrium and boundary conditions are satisfied consistently. The resulting formulation is applicable to beams with either increasing or decreasing stiffness distributions, provided that the flexural rigidity remains positive along the beam length. Numerical comparisons with results obtained from the KCW structural analysis program for cantilever and simply supported beams show excellent agreement, with differences in maximum displacement generally below about 2.5%. These comparisons confirm that the proposed analytical formulation accurately captures the influence of continuously varying flexural rigidity on beam deflection behavior.

The present formulation provides a transparent analytical benchmark for the response of non-prismatic beams and offers a useful reference for validating numerical and finite-element models. Although the current study focuses on displacement solutions, the approach provides a foundation for future extensions, including applications to shear-deformable beam theories, other stiffness variation profiles, and the development of stiffness, mass , and geometric matrices and load vectors for advanced structural analysis.

6. REFERENCES

1. Boley B.A., On the accuracy of the Bernoulli-Euler theory for beams of variable section. 1963. https://doi.org/10.1115/1.3636564
2. Eisenberger M., Explicit stiffness matrix for non-prismatic members. Computers & Structures, 20(1–3), 1984, pp. 715–720. https://doi.org/10.1016/0045-7949(85)90032-X
3. Banerjee J.R. and Williams F.W., Exact Bernoulli-Euler static stiffness matrix for a range of tapered beam-columns. International Journal for Numerical Methods in Engineering, 23(9), 1986, pp. 1615-1628. https://doi.org/10.1002/nme.1620230904
4. Tang X., Shape functions of tapered beam-column elements. Computers & Structures, 46(5), 1993, pp. 943–953. https://doi.org/10.1016/0045-7949(93)90155-7
5. Shooshtari A., & Khajavi R., An efficient procedure to find shape functions and stiffness matrices of non-prismatic Euler–Bernoulli and Timoshenko beam elements. European Journal of Mechanics A/Solids, 29(5), 2010, pp. 826–836. https://doi: 10.1016/j.euromechsol.2010.04.003
6. Valipour H.R., & Bradford M.A., A new shape function for tapered three-dimensional beams with flexible connections. Journal of Constructional Steel Research, 70, 2012, pp. 43–50. https://doi.org/doi: 10.1016/j.jcsr.2011.10.012
7. Soltani M., Asgarian B. & Mohri F., Finite element method for stability and free vibration analyses of non-prismatic thin-walled beams. Thin-Walled Structures, 82, 2014, pp. 245-261. https://doi.org/10.1016/j.tws.2014.04.012
8. Auricchio F., Balduzzi G. & Lovadina C., The dimensional reduction approach for 2D non-prismatic beam modelling: a solution based on Hellinger-Reissner principle. International Journal of Solids and Structures, 63, 2015, pp. 264-276. https://doi.org/10.1016/j.ijsolstr.2015.03.004
9. Ibrahim S. M., El-Aghoury A.A., Abbas H., Carrera E., Al-Saloum Y., & Almusalami T., Free vibration of tapered beams and plates based on unified beam theory. Journal of Vibration and Control, 22(10), 2016, pp. 2450–2465. https://doi.org/10.1177/1077546312473766
10. Bathe K.J., Finite Element Procedures, Prentice Hall, New Jersey, 1996.
11. Reddy J.N., 2006. Theory and analysis of elastic plates and shells. CRC press.
12. Hoang N.H., Plastic analysis of concrete-steel frame under static load. Dissertation, Hanoi Architectural University (in Vietnamese), 2020, pp. 1-178.